Cooling electrons from 1 K to 400 mK with V-based nanorefrigerators

O. Quaranta,[1, a)] P. Spathis,[1] F. Beltram,[1] and F. Giazotto[1, b)]
NEST, Istituto Nanoscienze-CNR and Scuola Normale Superiore, Piazza S. Silvestro 12, I-56127 Pisa, Italy

The fabrication and operation of V-based superconducting nanorefrigerators is reported. Specifically, electrons in an Al island are cooled thanks to hot-quasiparticle extraction provided by tunnel-coupled V electrodes. Electronic temperature reduction down to 400 mK starting from 1 K is demonstrated with a cooling power ~ 20 pW at 1 K for a junction area of $0.3\,\mu m^2$. The present architecture extends to higher temperatures refrigeration based on tunneling between superconductors and paves the way to the implementation of a multi-stage on-chip cooling scheme operating from above 1 K down to the mK regime.

The investigation of heat-transport at the nanoscale is currently the focus of an intense research effort[1]. In this context, solid-state refrigeration with an emphasis on superconducting tunnel structures is under the spotlight[1–8]. These superconducting refrigerators yielded the demonstration of sizable electron-temperature reductions[3,5,8] allowing to reach few tens of mK in optimized structures. These structures make a widespread use of Al as superconductor since this material makes it possible to fabricate high-quality tunnel junctions. On the other hand, however, Al limits the operation temperature of the coolers to a few hundreds of mK owing to its reduced critical temperature. Indeed the exploitation of a superconducting gap larger than that of Al is technologically challenging but would give the opportunity to extend this cooling method up to temperatures around or above 1K.

Here we report the fabrication and operation of V/AlO$_x$/Al all-superconducting refrigerators which demonstrate up to 60% reduction of electron temperature when operated at 1K, and provide an estimated cooling-power density of ~ 65 pW/μm^2. The ease of fabrication and the performance demonstrated here indicate the V-Al material combination as an ideal candidate for the implementation of on-chip cascaded refrigerators operating from above ~ 1 K down to the mK regime.

Figure 1(a) shows a scanning electron micrograph of a V-based double refrigerator along with a scheme of the measurement setup. A blow-up of the device which consists of a 15-nm-thick 600×1200 nm^2 Al island (S') tunnel-coupled to four V electrodes (S) is displayed in Fig. 1(b). Samples were fabricated by e-beam lithography and two-angle shadow-mask metal evaporation. Figure 1(c) shows a cross-section of the junctions. The barriers were obtained by oxidation of the Al layer in 100 mTorr of O$_2$ for 20' leading to tunnel junctions with $\sim 300\,\Omega\mu m^2$ specific resistance. Direct evaporation of V onto AlO$_x$ degrades junction quality, therefore a 15-nm-thick Al interlayer was first deposited to prevent direct contact between V and the oxide layer. The resulting junctions showed excellent stability against thermal cycling and reduced aging. The two lateral junctions (with
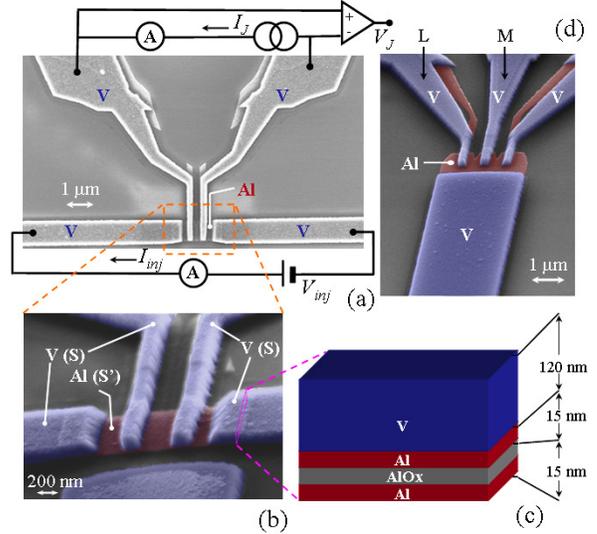
FIG. 1. (a) Scanning electron micrograph of a typical V-based nanorefrigerator along with a scheme of the measurement setup. I_{inj} is the current driven through the cooling junctions while I_J is that flowing through the Josephson thermometers. (b) A pseudo-color blow-up of the device core. V is the larger gap superconductor (S) acting as electron refrigerator. (c) Cross-section of the junctions (not to scale). (d) Pseudo-color micrograph of a reference structure (see text).

normal-state resistance $R_T \simeq 2$ kΩ each) are operated as electron coolers through current injection I_{inj},[1,4] whereas the two inner (with $R_T \simeq 2 - 3$ kΩ each) are used as Josephson thermometers to probe electron temperature in the island. The critical temperature of the Al island was $T_c^{S'} \simeq 1.55$ K whereas that of the 120/15-nm-thick V/Al bilayer was $T_c^S \simeq 4$ K. Figure 1(d) shows a reference structure that will be discussed later in the text. It consists of a few V tunnel junctions connected to a large-volume Al electrode.

Samples were characterized down to 280 mK in a filtered ^{3}He cryostat as follows. We first calibrated the Josephson thermometers[1,4], i.e., the series connection of the two central SIS' junctions (I denotes an insulator). To this end the dependence of the equilibrium Josephson critical current (I_c) on bath temperature (T_{bath}) was determined. These results were then used to convert the supercurrent amplitude under injection V_{inj} into an elec-
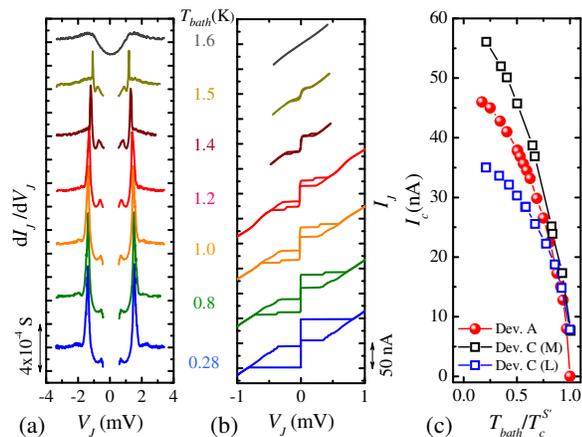
FIG. 2. (a) dI_J/dV_J vs V_J and (b) I_J vs V_J characteristics of thermometer junctions in device A at different T_{bath}. In (a) and (b) curves are vertically offset for clarity. (c) Equilibrium critical current I_c vs reduced temperature for three different junctions. Solid dots refer to device A, whereas open squares refer to the middle (M) and left (L) junctions in device C [see Fig. 1(d)].

FIG. 3. (a) I_J vs V_J characteristics of sample A thermometer junctions under several increasing V_{inj} at three different T_{bath}. The curves are horizontally offset for clarity. (b) Maximum critical current I_c vs V_{inj} at the same T_{bath}. Colored circles indicate V_{inj} values under which the characteristics shown in panel (a) were measured. The curves are vertically offset for clarity. Dashed lines in (a) and (b) indicate the equilibrium critical current at each corresponding temperature.

tronic temperature value in the Al island. In the following we shall present results obtained in two representative devices referred to as A and B.

Figure 2(a) shows the differential conductance dI_J/dV_J vs. voltage V_J for thermometer junctions in device A at different T_{bath} values. Curves are vertically offset for clarity. The two peaks appearing at higher voltage correspond to $V_J = \pm 2(\Delta_S + \Delta_{S'})/e$, while those appearing at lower energy to $V_J = \pm 2(\Delta_S - \Delta_{S'})/e$. This is the typical behavior of the tunneling characteristic between two different superconductors at finite temperature[9]. Here Δ_S ($\Delta_{S'}$) is the energy gap of V/Al (Al), and e is the electron charge. As the temperature is raised the two peaks merge, coinciding at temperatures larger than $T_c^{S'}$. The temperature evolution of the peaks closely follows the Bardeen-Cooper-Schrieffer (BCS) behavior[9]. From the low-temperature voltage position of the peaks we deduced $\Delta_S \simeq 580$ μeV and $\Delta_{S'} \simeq 200$ μeV.

The corresponding I_J vs V_J characteristics are displayed in Fig. 2(b). Junctions exhibit a hysteretic dc Josephson effect, as expected for underdamped tunnel weak links[9]. At intermediate temperatures a finite-bias step is observed which stems from a slight asymmetry between the junctions which leads to a non simultaneous switching to the resistive state. The Josephson coupling persists up to $\simeq 1.55$ K. Above this temperature the island is driven into the normal state.

The full temperature evolution of the equilibrium supercurrent at $V_J = 0$ for the same junctions is shown in Fig. 2(c) (solid dots). In particular, I_c monotonically increases by reducing T_{bath} without showing saturation even at the lowest temperatures. This behavior markedly differs from the Ambegaokar-Baratoff prediction[10] and
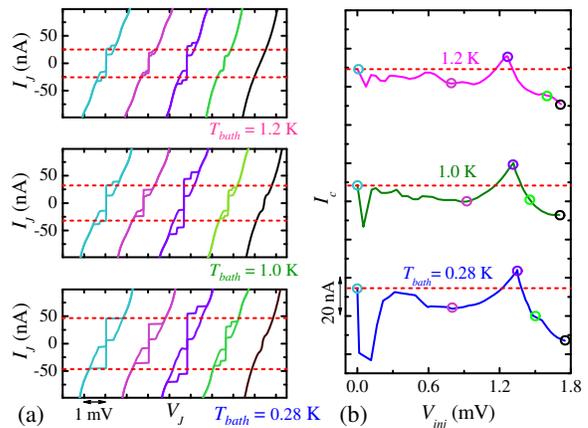
is expected for tunnel junctions embedding an interlayer like the present[11,12]. In order to validate our temperature calibration and rule out spurious overheating in the small island we also measured the $I_c(T_{bath})$ dependence on similar junctions fabricated on a large-volume Al electrode, i.e., device C shown in Fig. 1(d) (open squares). Besides showing different I_c, the junctions exhibit the same temperature dependence when normalized at each corresponding maximum supercurrent thus confirming the role of the Al interlayer.

Figure 3(a) shows the I_J vs V_J characteristics for thermometers in sample A with increasing values of V_{inj}. Curves are horizontally offset for clarity; each panel refers to a different T_{bath}. The evolution of the Josephson supercurrent upon increasing V_{inj} is non-monotonic: at all measured temperatures I_c is initially suppressed, then it increases and even exceeds the equilibrium value. This latter behavior occurs thanks to hot-quasiparticle extraction provided by V reservoirs which *cools* the electron population in the island[1,4]. Further increase of V_{inj} leads to a decay of I_c then followed by suppression of the supercurrent for larger injection voltage.

The full evolution of I_c under V_{inj} is shown in Fig. 3(b) for the same T_{bath} values. Colored circles indicate the V_{inj} values at which the characteristics shown in Fig. 3(a) were measured. Supercurrent enhancement is clearly observable even at 1.2 K. Such a nonmonotonic behavior of the Josephson current closely resembles that reported and extensively discussed in Ref. [4], and originates from the presence of a floating superconductor coupled to biased superconducting electrodes.

Figure 4(a) shows I_c vs T_{bath} (open squares) for both samples. As anticipated [see also Fig. 2(c)], I_c increases monotonically upon lowering T_{bath}, and at 280 mK ex-
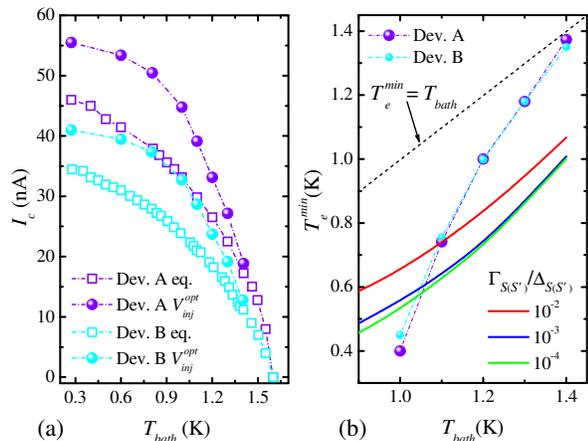
FIG. 4. (a) I_c vs T_{bath} for device A and B at the equilibrium, i.e., at $V_{inj} = 0$ (open squares), and at V_{inj}^{opt} (solid dots). (b) Minimum electron temperature T_e^{min} at V_{inj}^{opt} vs T_{bath} for both samples (solid dots). Dash-dotted lines are guides to the eye. Full lines are the prediction for an ideal SIS'IS refrigerator with the same parameters as in our samples calculated for different $\Gamma_{S(S')}$ values. Dashed line represents $T_e^{min} = T_{bath}$.

hibits values as large as ~ 35 nA and ~ 46 nA for sample A and B, respectively. For comparison, the maximum I_c at the optimized injection voltage V_{inj}^{opt}, i.e., that which maximizes the supercurrent at each T_{bath}, is also displayed (solid dots). Below $\simeq 1.3$ K the out-of-equilibrium supercurrent exceeds that at equilibrium, attaining ~ 42 nA and ~ 56 nA in sample A and B, respectively, at 280 mK.

The minimum electron temperature T_e^{min} achieved under injection in the island at different T_{bath} values is shown in Fig. 4(b) (solid dots). T_e^{min} was determined by comparing the maximum I_c at V_{inj}^{opt} with the equilibrium values [panel (a)]. A dramatic cooling is achieved at 1 K where T_e^{min} values as low as ~ 400 mK and ~ 450 mK in sample A and B, respectively, were obtained which correspond to up to 60% temperature reduction. Moreover, substantial cooling is obtained even at 1.2 K where $T_e^{min} \sim 1$ K. At lower T_{bath} we cannot determine T_e^{min} owing to the lack of a temperature calibration below 280 mK.

Insight into the operation of the refrigerator can be gained based on a simple model which includes energy relaxation in the island and the heat flux originating from injection. Although rather idealized, this analysis allows us to grasp the essential features of our system. Under bias voltage V_{inj} the heat current flowing from S' to the S electrodes is given by[1,4] $\dot{Q} = 2(e^2 R_T)^{-1} \int d\varepsilon \varepsilon \mathcal{N}_S(\tilde{\varepsilon}) \mathcal{N}_{S'}(\varepsilon)[f_0(\varepsilon, T_e^{S'}) - f_0(\tilde{\varepsilon}, T_e^S)]$, where $\tilde{\varepsilon} = \varepsilon - eV_{inj}/2$, $f_0(\varepsilon, T)$ is the Fermi-Dirac function at temperature T, and $\mathcal{N}_{S,S'}(\varepsilon) = |\text{Re}[(\varepsilon + i\Gamma_{S,S'})/\sqrt{(\varepsilon + i\Gamma_{S,S'})^2 - \Delta_{S,S'}^2(T_e^{S,S'})}]|$ is the smeared BCS density of states where $\Gamma_{S,S'}$ accounts for nonidealities in S(S').[1,5] We consider a transport regime where

strong quasiparticle interaction in S' forces the electron system to retain a thermal *quasiequilibrium* at temperature $T_e^{S'}$ differing in general from T_{bath}. The actual $T_e^{S'}$ upon current injection is the result of the competition between $\dot{Q}$ and other relaxation mechanisms transferring energy into S'. At low T_{bath} the predominant contribution comes from electron-phonon interaction $\dot{Q}_{e-ph}^{S'}$ [see Eq. (2) of Ref. [13]] which allows energy exchange between electrons and lattice phonons[1,13]. The steady-state $T_e^{S'}$ is obtained by solving the energy-balance equation $\dot{Q}(V_{inj}, T_{bath}, T_e^{S'}) + \dot{Q}_{e-ph}^{S'}(T_{bath}, T_e^{S'}) = 0$.

Solid lines in Fig. 4(b) represent T_e^{min} as obtained from the solution of the balance equation for different values of $\Gamma_{S(S')}$. In particular an increase of $\Gamma_{S(S')}$ leads for each T_{bath} to a reduced cooling which stems from enhanced heating originating from subgap current in tunnel junctions[1,5,14]. At higher T_{bath} values the experimental data deviate from the calculations which predict a lower T_e^{min}, whereas the agreement is improved for $T_{bath} \leq 1.1$ K. The nature of our junctions which include an (Al) interlayer might explain the deviation from this rather simplified model that actually holds for ideal SIS' junctions.

We should finally comment on the available cooling power. Based on the expression for $\dot{Q}$ we estimate that our structures provide a maximum $\dot{Q}$ of ~ 20 pW at 1 K corresponding to ~ 65 pW/μm^2 areal cooling-power density. This value can be increased by either lowering the junctions specific resistance or by optimizing the thickness of the Al interlayer.

In conclusion, we have reported the fabrication and operation of V-based nanorefrigerators. These coolers show a significant temperature reduction, i.e., up to 60% when operating at 1 K, and provide an areal cooling-power density of ~ 65 pW/μm^2. Furthermore, the fabrication protocol yields junctions with excellent stability and reduced aging. Our results pave the way to the implementation of a solid-state multi-stage refrigeration platform which would enable on-chip cooling from the base temperature of a ^{4}He cryostat down to the mK regime.

[1] F. Giazotto, T. T. Heikkilä, A. Luukanen, A. M. Savin, and J. P. Pekola, Rev. Mod. Phys. **78**, 217 (2006).
[2] M. Nahum, T. M. Eiles, and J. M. Martinis, Appl. Phys. Lett. **65**, 3123 (1994).
[3] M. M. Leivo, J. P. Pekola, and D. V. Averin, Appl. Phys. Lett. **68**, 1996 (1996).
[4] S. Tirelli, A. M. Savin, C. Pascual Garcia, J. P. Pekola, F. Beltram, and F. Giazotto, Phys. Rev. Lett. **101**, 077004 (2008).
[5] J. P. Pekola, T. T. Heikkilä, A. M. Savin, J. T. Flyktman, F. Giazotto, and F. W. J. Hekking, Phys. Rev. Lett. **92**, 056804 (2004).
[6] S. Kafanov, A. Kemppinen, Yu. A. Pashkin, M. Meschke, J. S. Tsai, and J. P. Pekola, Phys. Rev. Lett. **103**, 120801 (2009).
[7] A. J. Manninen, J. K. Suoknuuti, M. M. Leivo, and J. P. Pekola, Appl. Phys. Lett. **74**, 3020 (1999).
[8] A. M. Clark, A. Williams, S. T. Ruggiero, M. L. van den Berg, and J. N. Ullom, Appl. Phys. Lett. **84**, 625 (2004).

[9] M. Tinkham, *Introduction to Superconductivity*, 2nd Ed. (McGraw-Hill, New York, 1996).

[10] V. Ambegaokar and A. Baratoff, Phys. Rev. Lett. **10**, 486 (1963); **11**, 104(E) (1963).

[11] A. A. Golubov, E. P. Houwman, J. G. Gijsbertsen, V. M. Krasnov, J. Flokstra, H. Rogalla, and M. Yu. Kupriyanov, Phys. Rev. B **51**, 1073 (1995).

[12] G. Brammertz, A. Poelaert, A. A. Golubov, P. Verhoeve, A. Peacock, and H. Rogalla, J. Appl. Phys. **90**, 355 (2001).

[13] A. V. Timofeev, C. Pascual Garcia, N. B. Kopnin, A. M. Savin, M. Meschke, F. Giazotto, and J. P. Pekola, Phys. Rev. Lett. **102**, 017003 (2009).

[14] S. Rajauria, P. Gandit, T. Fournier, F. W. J. Hekking, B. Pannetier, and H. Courtois, Phys. Rev. Lett. **100**, 207002 (2008).